Eur J Nucl Med Mol Imaging (2016) 43:1653–1663
DOI 10.1007/s00259-016-3332-6

ORIGINAL ARTICLE

[^{11}C]TASP457, a novel PET ligand for histamine H_3 receptors in human brain

Yasuyuki Kimura[1] · Chie Seki[1] · Yoko Ikoma[1] · Masanori Ichise[1] · Kazunori Kawamura[1] · Keisuke Takahata[1] · Sho Moriguchi[1] · Tomohisa Nagashima[1] · Tatsuya Ishii[1] · Soichiro Kitamura[1] · Fumitoshi Niwa[1] · Hironobu Endo[1] · Makiko Yamada[1] · Makoto Higuchi[1] · Ming-Rong Zhang[1] · Tetsuya Suhara[1]

Received: 28 September 2015 / Accepted: 7 February 2016 / Published online: 23 February 2016
© Springer-Verlag Berlin Heidelberg 2016

Abstract
Purpose The histamine H_3 receptors are presynaptic neuroreceptors that inhibit the release of histamine and other neurotransmitters. The receptors are considered a drug target for sleep disorders and neuropsychiatric disorders with cognitive decline. We developed a novel PET ligand for the H_3 receptors, [^{11}C]TASP0410457 ([^{11}C]TASP457), with high affinity, selectivity and favorable kinetic properties in the monkey, and evaluated its kinetics and radiation safety profile for quantifying the H_3 receptors in human brain.
Methods Ten healthy men were scanned for 120 min with a PET scanner for brain quantification and three healthy men were scanned for radiation dosimetry after injection of 386 ± 6.2 MBq and 190 ± 7.5 MBq of [^{11}C]TASP457, respectively. For brain quantification, arterial blood sampling and metabolite analysis were performed using high-performance liquid chromatography. Distribution volumes (V_T) in brain regions were determined by compartment and graphical analyses using the Logan plot and Ichise multilinear analysis (MA1). For dosimetry, radiation absorbed doses were estimated using the Medical Internal Radiation Dose scheme.
Results [^{11}C]TASP457 PET showed high uptake (standardized uptake values in the range of about 3 – 6) in the brain and fast washout in cortical regions and slow washout in the pallidum. The two-tissue compartment model and graphical analyses estimated V_T with excellent identification using 60-min scan data (about 16 mL/cm^3 in the pallidum, 9 – 14 in the basal ganglia, 6 – 9 in cortical regions, and 5 in the pons), which represents the known distribution of histamine H_3 receptors. For parametric imaging, MA1 is recommended because of minimal underestimation with small intersubject variability. The organs with the highest radiation doses were the pancreas, kidneys, and liver. The effective dose delivered by [^{11}C]TASP457 was 6.9 μSv/MBq.
Conclusion [^{11}C]TASP457 is a useful novel PET ligand for the investigation of the density of histamine H_3 receptors in human brain.

Keywords PET quantification · Histamine H_3 receptors · [^{11}C]TASP0410457 · [^{11}C]TASP457 · Dosimetry

Introduction

Histamine H_3 (H_3) receptors are found in presynaptic histaminergic neurons and act as autoreceptors regulating histamine turnover by feedback inhibition of histamine synthesis and release [1]. H_3 receptors also act as inhibitory heteroreceptors which presynaptically inhibit the release of a number of other neurotransmitters including dopamine, GABA, acetylcholine and serotonin [2]. H_3 receptors are expressed prominently in the basal ganglia, hippocampus, and neocortex [3], and are considered a drug target for sleep disorders and neuropsychiatric disorders with cognitive deficits [4]. Thus, PET imaging using a suitable radioligand for H_3 receptors allows investigation of the role of this receptor in

✉ Yasuyuki Kimura
y-kimura@nirs.go.jp

✉ Masanori Ichise
ichisem@nirs.go.jp

[1] Molecular Imaging Center, National Institute of Radiological Sciences, 4-9-1 Anagawa, Inage-ku, Chiba 263-8555, Chiba, Japan

various disorders and also facilitates development of drugs targeting H_3 receptors using H_3 receptor occupancy.

To date, there have been two PET ligands available for quantifying H_3 receptors in human brain. GlaxoSmithKline and Imperial College developed the first clinically used PET ligand for H_3 receptors ([^{11}C]GSK189254) and measured occupancy after oral administration of unlabeled H_3 antagonists, GSK189254 [5] and GSK239512 [6], in healthy humans. AstraZeneca and the Karolinska Institute used the same ligand to evaluate the time-course of H_3 receptor occupancy after a single dose of the H_3 antagonist, AZD5213 [7]. Merck and University Hospital Gasthuisberg Leuven developed another PET ligand ([^{11}C]MK-8278) and measured occupancy after administration of the H_3 inverse agonists, MK-0249 and MK-3134 [8].

However, using two of the PET ligands discussed above there is some difficulty in the quantification of H_3 receptors in human brain. First, [^{11}C]GSK189254 has an extremely high affinity for H_3 receptors in humans (K_D 0.08 nM) [9]. Its slow kinetics in the brain limits the accuracy and precision of PET quantification of H_3 binding density, especially in high-density regions such as the globus pallidus and striatum [5]. Second, [^{11}C]MK-8278 has shown large test–retest variability, especially in the high-density regions [8]. In the putamen and caudate, the test–retest variability of total distribution volume values are large (more than 15 %), which can be explained by low statistics in the plasma curve at times beyond 60 min.

Recently, we labelled TASP0410457, a compound that has high affinity and selectivity for H_3 receptors, with ^{11}C ([^{11}C]TASP457). This compound showed favorable kinetics in monkeys for quantification H_3 receptors [10]. The IC_{50} of TASP0410457 for [^{3}H]*N*-α-methylhistamine, an agonist selective for H_3 receptors, was 1.8 nM in monkeys. Negligible affinity was shown for other receptors with 379 nM IC_{50} for σ_1 receptors (210 times higher selectivity for H_3 than for σ_1 receptors) and >1,000 nM for 67 other receptors and transporters [10]. Fast and high radioligand uptake (standardized uptake value about 3) was found in monkeys, and adequate washout in the brain and good separation of time–activity curves between high-density and low-density areas. With H_3 blocked by administration of the H_3 antagonist ciproxifan, the time–activity curves became uniform across brain regions, confirming good specific to nonspecific ratios of the radioligand activity. Thus, [^{11}C]TASP457 appears to be a good candidate for quantification of H_3 receptors in the human brain.

The purposes of this study were to evaluate the kinetics of [^{11}C]TASP457 for quantifying H_3 receptors in the human brain and to evaluate the radiation safety profile of the ligand. We conducted a first-in-human PET study with arterial blood sampling and metabolite analysis and applied compartment model analyses and graphical analyses to evaluate the accuracy of PET quantification of H_3 receptors in humans. We also performed whole-body PET scans to estimate the effective dose of [^{11}C]TASP457.

Materials and methods

Subjects

Ten healthy male volunteers (body weight 62 ± 7 kg, age 25 ± 4 years) were enrolled for brain quantification and three healthy male volunteers (body weight 61 ± 4 kg, age 25 ± 1 years) for radiation dosimetry. All subjects were free of medical and neuropsychiatric illnesses on the basis of their medical and occupational history, physical examination, standard blood tests including a complete blood cell count and serum chemistry, and urinalysis. Blood tests were repeated 2 h after injection of the radioligand. The study was approved by the Radiation Drug Safety Committee and the Institutional Review Board of the National Institute of Radiological Sciences of Japan, and was performed in accordance with the ethical standards laid down in the 1964 Declaration of Helsinki and its later amendments. All subjects gave written informed consent prior to their inclusion in the study. The study was registered with the University Hospital Medical Information Network Clinical Trials Registry (UMIN000011422).

Radioligand preparation

[^{11}C]TASP457 was prepared by O-alkylation of the 2-pyridone-containing precursor (desmethyl TASP457) using [^{11}C]methyl triflate. [^{11}C]Methyl triflate was prepared and trapped in the mixture solution of desmethyl TASP457 (1.0 mg) and cesium carbonate (10 mg) in *N*,*N*-demethylformamide (DMF, 0.3 mL) on heating at 100 °C, and the mixture solution was heated at 100 °C for 1 min. The synthesized [^{11}C]TASP457 was purified using preparative high-performance liquid chromatography (HPLC; Jasco, Tokyo, Japan) on a XBridge Prep C18 column (5 μm, 10 × 250 mm; Waters, Milford, MA) with a mobile phase consisting of acetonitrile/50 mmol/L phosphoric acid (130/370, vol/vol) at a flow rate of 4.0 mL/min. The radiochemical purity of [^{11}C]TASP457 was more than 95 %, and the specific activity was more than 37 GBq/μmol at the time of administration.

Brain PET scans

After intravenous injection of [^{11}C]TASP457 (386 ± 6.2 MBq , specific activity 92 ± 32 GBq/μmol, corresponding to 4.9 ± 2.4 nmol, 2.0 ± 1.0 μg, TASP457), three-dimensional

dynamic images were acquired on a PET camera (Eminence SET-3000GCT/X; Shimadzu, Kyoto, Japan) for 120 min with 39 frames of increasing duration from 10 s to 5 min (10 s × 6, 20 s × 3, 1 min × 5, 3 min × 4, and 5 min × 20). All PET images were reconstructed using the filtered back-projection method (gaussian filter, kernel 5 mm; reconstructed in-plane resolution 7.5 mm at full-width at half-maximum; voxel size 2 × 2 × 2.6 mm) with correction for attenuation, randoms and scatter. Head motion during the scans was corrected on the emission images after attenuation correction with μ-maps realigned to each frame of the emission images [11]. The largest corrected movements were 4.4 mm in the z-axial direction and 4.9 degrees of yaw-rotation.

Measurement of [^{11}C]TASP457 in plasma

Arterial blood samples were taken manually 35 times after injection of radioligand to obtain arterial input functions (at 10-s intervals up to 120 s, at 30-s intervals up to 3 min, at 1-min intervals up to 10 min, at 12, 15, 20, 25 and 30 min, and at 10-min intervals up to 120 min). Each blood sample was centrifuged to obtain plasma and blood cell fractions, and the concentrations of radioactivity in whole blood and plasma were measured. The plasma-free fraction was measured by ultrafiltration (Centrifree, Merck Millipore, Billerica, MA).

The fractions of the parent and its radiometabolites in plasma were determined by HPLC from eight samples in each subject (at 3, 10, 20, 30, 50, 70, 90 and 120 min). The supernatant of the centrifuged samples was subjected to radio-HPLC analysis (CAPCELL PAK C18 5 μm, 10 × 150 mm, column; Shiseido Co. Ltd., Tokyo, Japan). Acetonitrile (90 %; A) and phosphoric acid (0.01 M B) were used as mobile phases (35/65 A/B) at a flow rate of 6.0 mL/min.

Since radioactivity of the metabolite was low and its radioactivity decayed quickly with a half life of about 20 min, the parent fraction was determined at 90 min in only half of the subjects and at 30 – 70 min in the remaining subjects depending on the quality of the radiochromatogram. After initial evaluation of quantification with individual parent fractions, to improve the statistical quality of the input functions for further evaluation of the region of interest (ROI) analysis and parametric imaging, we created a mean parent fraction curve from the average of the parent fractions of all subjects at each time-point.

Brain image analysis

T1-weighted MR images acquired with a 3-T MRI scanner (Verio, Siemens, Germany; TE 1.9 ms, TR 2,300 ms, TI 900 ms, flip angle 9°, field of view 250 mm, acquisition matrix 256 × 256, slice thickness 1 mm) were coregistered to the corresponding PET images. Both MR and PET images were then spatially normalized to standard anatomic orientation (MNI152 standard space; Montreal Neurological Institute, Montreal, QC, Canada) based on transformation parameters from the MR images. A template of preset volumes of interest was applied to the spatially normalized PET images to extract time–activity curves for the following 15 ROIs: frontal (432 cm^3), cingulate (28 cm^3), parietal (247 cm^3), occipital (172 cm^3), temporal cortices (251 cm^3), hippocampus (15 cm^3), amygdala (3.7 cm^3), caudate (16 cm^3), putamen (17 cm^3), pallidum (4.6 cm^3), thalamus (17 cm^3), hypothalamus (1.3 cm^3), substantia nigra (0.8 cm^3), cerebellum (195 cm^3), and pons (1.8 cm^3). All image and kinetic analyses were performed using PMOD, version 3.6 (PMOD Technologies Ltd., Zurich, Switzerland).

Brain kinetic analysis

Regional total distribution volumes (V_T) [12] were estimated using compartment analyses and graphical analyses using the arterial input function. Tissue and blood data from the 90-min scan in five subjects whose parent fractions were obtained successfully at 90 min were used for the initial evaluation of quantification. For compartment analyses, the optimal compartment model (one-tissue or two-tissue) was chosen on the basis of the Akaike information criterion (AIC) [13], model selection criterion (MSC) [14], goodness of fit assessed with F statistics [15], and the identifiability of V_T, which is the ratio of the standard error (SE) of V_T divided by V_T [16]. For graphical analyses, the Logan plot [17, 18] and Ichise multilinear analysis (MA1) [19] were used to estimate V_T in two ways: ROI analysis and parametric imaging, which allows voxel-based analysis. For the one-tissue and two-tissue compartment models, fractional blood volume was fixed at 0.05. For graphical analyses, blood volume was not considered.

To investigate the effect of scan duration on the estimation of V_T, truncated PET data for shorter scan durations by 10 min stepwise from 90 min down to 40 min for graphical analyses and to 30 min for compartment model analysis were analyzed. Based on the initial analysis, we suspected that the radiometabolites of [^{11}C]TASP457 slowly enter the brain. We evaluated the correlation of V_T values between the two-tissue compartment and dual-input compartment models, the latter accounting for the contribution of the metabolite brain activity. The applied dual-input compartment model was a six-parameter model assuming no specific binding of radiometabolites and no conversion of the parent to radiometabolites in tissue [14, 20].

Body PET scan

After intravenous injection of [^{11}C]TASP457 (190 ± 7.5 MBq, specific activity 160 ± 14 GBq/μmol, corresponding to 1.2 ± 0.1 nmol, 0.5 ± 0.03 μg. TASP457; ^{11}C half-life 20.4 min), 3-D serial PET images from the head to the upper thighs were

acquired using a Biograph mCT flow PET scanner (Siemens, Munich, Germany), cross-calibrated with a well scintillation counter using a physical calibration phantom. Each subject was scanned on a continuously moving bed from the head to the upper thighs repeatedly for a total scan time of 123 min (1.2 – 10 mm/s for 1,200-mm field of view, 13 frames: three frames 2 min, two frames 3.6 min, three frames 7.6 min, and five frames 16.4 min). Intervals between frames for the bed moving back to the head position were between 11 s and 36 s. All PET images were reconstructed with the filtered back-projection method (gaussian filter, kernel 5 mm) and were corrected for attenuation based on the CT images, for randoms using the delayed coincidence counting method, and for scatter using the single-scatter simulation method.

Body image analysis

Analysis of body images was based on a previously reported method with slight modification [21]. Briefly, source organs were chosen from visually identifiable organs on the PET images. In each subject, source organ ROIs were drawn on a slice-by-slice basis on the CT images registered with the PET images and adjusted to visually circumscribe most of the activity within the respective source organ of the PET images. For the skeleton, ROIs were drawn only on the bodies of the lumbar vertebrae.

Calculation of residence time

Calculation of residence time was also based on a previously reported method [21]. The residence time in each source organ was calculated as the area under the curve of the time–activity curve, which was created after removing the decay correction and expressed as percentage of total activity in the body measured on PET (about 90 % of injected activity). The time–activity curves were created with time information, which was estimated from the starting time of each frame, and the distance from the top of the field of view to the center of each ROI divided by the bed speed of each frame. The area under the curve to the end of imaging was calculated using the trapezoidal method, and from the end to infinity was calculated by assuming that further decline in radioactivity occurred only by physical decay without any biological clearance.

The residence time of all red marrow in the body was estimated from that of the lumbar vertebrae. To conservatively estimate the radiation absorbed doses, we assigned all radioactivity in the lumbar vertebrae to the red marrow. Because the mass of the red marrow in the lumbar vertebrae is 12.3 % of the mass of all red marrow in the body (ICRP publication 89), the residence time in the red marrow in the entire body was calculated by multiplying that of the lumbar vertebrae by 100/12.3. To conservatively calculate the residence time of the remainder of the body, we assumed that there was no excretion of ^{11}C from the body. The residence time of all source organs was summed and subtracted from the fixed theoretical value of $T_{1/2}/\ln 2$, which equals 0.490 h for ^{11}C.

Estimation of absorbed dose

Radiation absorbed doses were calculated based on the Medical Internal Radiation Dose scheme by entering the residence times of each subject for each source organ into OLINDA/EXM 1.1 software [22] for a 70-kg adult male. OLINDA/EXM calculated an effective dose based on the recommendation in ICRP Publication 60.

Results

Pharmacological effects

[^{11}C]TASP457 caused no subjective symptoms during or after the 2-h scans. In addition, no effects on any of the blood tests performed 2 h after radioligand injection were noted, except in one subject who showed a slight increase in serum total bilirubin from 0.9 mg/dL at baseline to 1.6 mg/dL, which was not seen in the other subjects.

Plasma analysis

Plasma radioactivity showed fast washout (Fig. 1a). One major radiometabolite of [^{11}C]TASP457, which was much more hydrophilic than the parent radioligand, appeared slowly in the plasma (Fig. 1b, c). The metabolism of the radioligand was slow such that about 70 % of the radioactivity was unmetabolized at 90 min. Individual variation in the parent fraction was modest (less than 8 % coefficient of variation up to 70 min and 16 % up to 90 min). The plasma-free fraction of [^{11}C]TASP457 was 24 ± 3 %.

Brain uptake

After injection of ^{11}C-TASP457, the peak uptake of brain radioactivity was very adequate (standardized uptake values in the range of about 3 – 6). The washout was fast in cortical regions and the slowest in the pallidum, where the density of H_3 receptors is highest (Fig. 2).

Brain kinetic analysis

V_T was well identified using the two-tissue compartment model, the Logan plot and MA1 with 60-min scan data, and its rank was consistent with the known distribution of H_3 receptors. For the compartment model analysis with 90-min data in five subjects whose parent fractions were successfully measured at 90 min, the two-tissue compartment model fitted the

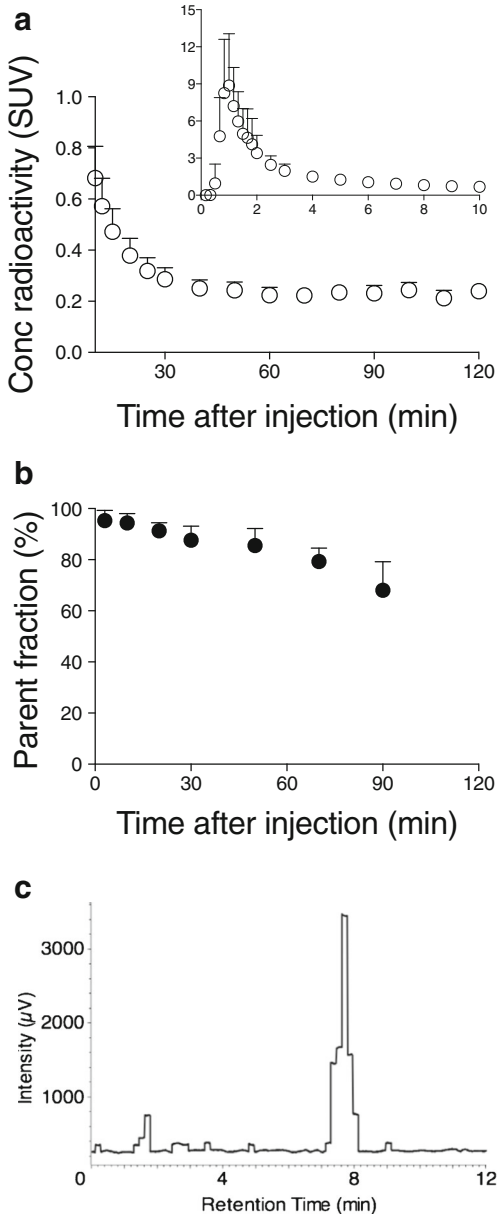

Fig. 1 Concentration of radioactivity and fraction of parent compound in arterial plasma after injection of [^{11}C]TASP457. **a** Concentration of radioactivity in plasma. Values from 0 to 10 min and 10 to 120 min are shown in the two graphs with different *y*-axis ranges. **b** Fraction of parent compound in plasma. Data are means ± SD from ten subjects. **c** Representative radiochromatogram at 20 min after injection of [^{11}C]TASP457

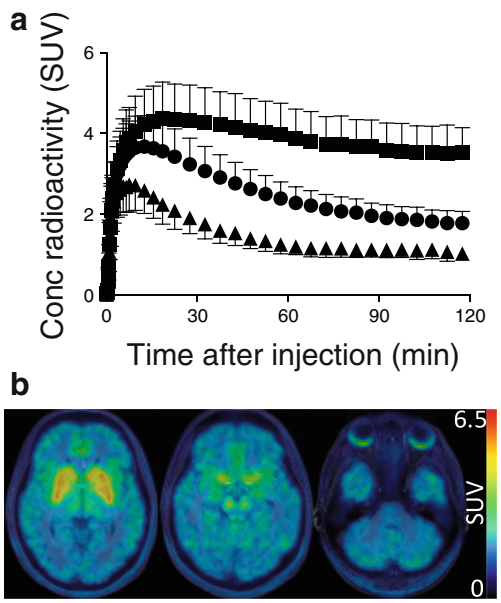

Fig. 2 **a** Average time-course of radioactivity in the pallidum (*squares*), cingulate (*circles*) and pons (*triangles*) after injection of [^{11}C]TASP457. Data are means ± SD from ten subjects. **b** Representative imaging in a healthy subject injected with [^{11}C]TASP457. Transaxial PET images were obtained by averaging from 30 to 120 min at the level of striatum (*left*), midbrain (*center*) and pons (*right*) and were fused with corresponding T1-weighted MR images

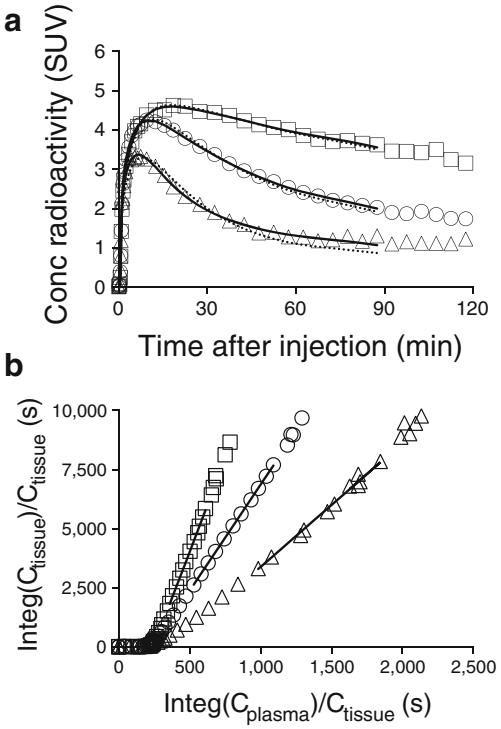

Fig. 3 **a** Concentrations of radioactivity in the pallidum (*squares*), cingulate (*circles*) and pons (*triangles*) after injection of [^{11}C]TASP457 fitted with one-tissue compartment model (*dotted lines*) and the two-tissue compartment model (*solid lines*). **b** Curve fitting of the 90-min data by the Logan plot in the pallidum (*squares*), cingulate (*circles*), and pons (*triangles*) in the same subject. The plots are linear after 30 min (*t**)

time–activity curves better than the one-tissue compartment model (Fig. 3a). AIC, MSC and *F*-test indicated that two-tissue fitting (AIC/MSC 412 ± 31/5.9 ± 1.1) was superior to one-tissue fitting (AIC/MSC 472 ± 18/4.2 ± 0.8) in all regions for all subjects ($p < 0.001$ in *F*-test for all regions). However, the estimation of V_T was not stable (%SE >10 %) using the two-tissue compartment model in 5 of 75 regions. With data from shorter scans, two-tissue analyses estimated V_T values stably for all regions. Estimated V_T values

with the two-tissue compartment model did not change from 40-min data to 80-min data, but slightly increased with 90-min data (Fig. 4a). V_T values were not well estimated in a significant number of regions with data from scans shorter than 40 min. The mean identifiability of V_T values was good for 50-min data to 80-min data (mean %SE <2 %).

For graphical analyses, the Logan and MA1 graphical plots became linear after $t^* = 30$ min in all regions in all subjects (Fig. 3b). The clearly non-zero t^* values of 30 min agreed with the findings that the kinetics of ^{11}C-TASP457 were better described by the two-tissue compartment model than by the one-tissue compartment model in which t^* is zero. V_T values estimated with the Logan plot and MA1 were stable for the data from 40 min to 70 min but V_T values gradually increased for data from scans beyond 70 min (Fig. 4b).

The slight increases in V_T with the two-tissue compartment model and MA1 with the longer scan durations might have been due to the metabolite slowly entering the brain [23]. Based on the time stability analysis, we decided that 60 min was the appropriate scan duration for this ligand. With the 60-min data from eight subjects, V_T values were well estimated with the two-tissue compartment model (%SE <10 % in 117 of 120 regions), which provided a better fit than the one-tissue compartment model in all regions. V_T values were the highest

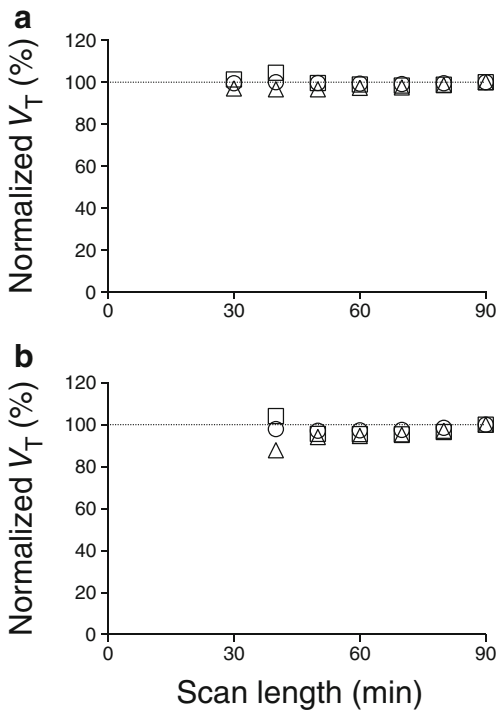

Fig. 4 V_T as a function of scan duration. V_T values were estimated in the pallidum (*squares*), cingulate (*circles*) and pons (*triangles*) with the two-tissue compartment model (**a**) and MA1 (**b**) with scan duration truncated from 90 to 40 min. V_T values are expressed as percentage of the V_T values estimated with the 90-min data. *Dotted lines* indicate 100 % of the normalized V_T value

in the pallidum (about 16 mL/cm^3), followed by striatal regions (about 11 – 14 mL/cm^3), hypothalamus, substantia nigra, and amygdala (about 9 – 11 mL/cm^3), cingulate cortex, hippocampus and thalamus (about 7 – 9 mL/cm^3), the other cortical regions including cerebellum (about 6 mL/cm^3), and pons (about 5 mL/cm^3 Fig. 5a). The rank order of the V_T values was consistent with the known distribution of H_3 receptors [5, 24]. V_T values determined with the Logan plot and MA1 were well correlated with those estimated with the two-tissue compartment model with slight underestimation ($r^2 = 1.00$ for both models, Fig. 5b, c). The intersubject coefficient of variance for V_T values was less than 15 % for all models in all regions except the very small regions for the two-tissue compartment model (21 % and 16 % for the hypothalamus and substantia nigra, respectively).

Considering radiometabolites in the brain, the dual-input compartment model with 90-min scan data from five subjects was able to estimate V_T (identifiability, mean ± SD %SE8.7 ± 8.4). Scans shorter than 90 min did not provide enough data points for the six-parameter dual-input model analysis. The two-tissue model V_T values from the 60-min scan data without consideration of radiometabolites in the brain correlated very well with the dual-input V_T values from the 90-min scan data ($r^2 = 0.98$; Fig. 6).

To improve statistical quality of the input functions, an alternative approach to quantification was applied using a population-mean parent fraction curve from the average of parent fractions of all subjects at each time point. The V_T values estimated with the mean parent fraction matched very well with those estimated with individual parent fractions for the 90-min and 60-min scan data ($r^2 = 0.99$ and 1.00, respectively; Fig. 7).

V_T values from parametric images estimated using the Logan plot were underestimated compared with those estimated using ROI-based analysis, especially in small regions (16 %, 17 % and 26 % in hypothalamus, pons and substantia nigra, respectively; Fig. 8a). On the other hand, V_T values from parametric images estimated using MA1 did not show such underestimation except in the pons (17 %) (Fig. 8b). Intersubject variabilities of regional V_T values estimated from parametric images were similar (<13 % coefficient of variance) to those from ROI analysis except in the substantia nigra (29 % coefficient of variance).

Dosimetry

Brain, thyroid, lungs, heart, liver, pancreas, spleen, stomach, large intestine, small intestine, kidneys, skeleton, and urinary bladder were visually identified on the PET images and treated as sources of radioactivity for dosimetry calculations (Fig. 9). The lungs had the highest uptake, with a maximum of 46 % of injected activity at 1 min after injection, and showed rapid washout (Fig. 10). Rapid washin and washout (within 5 min

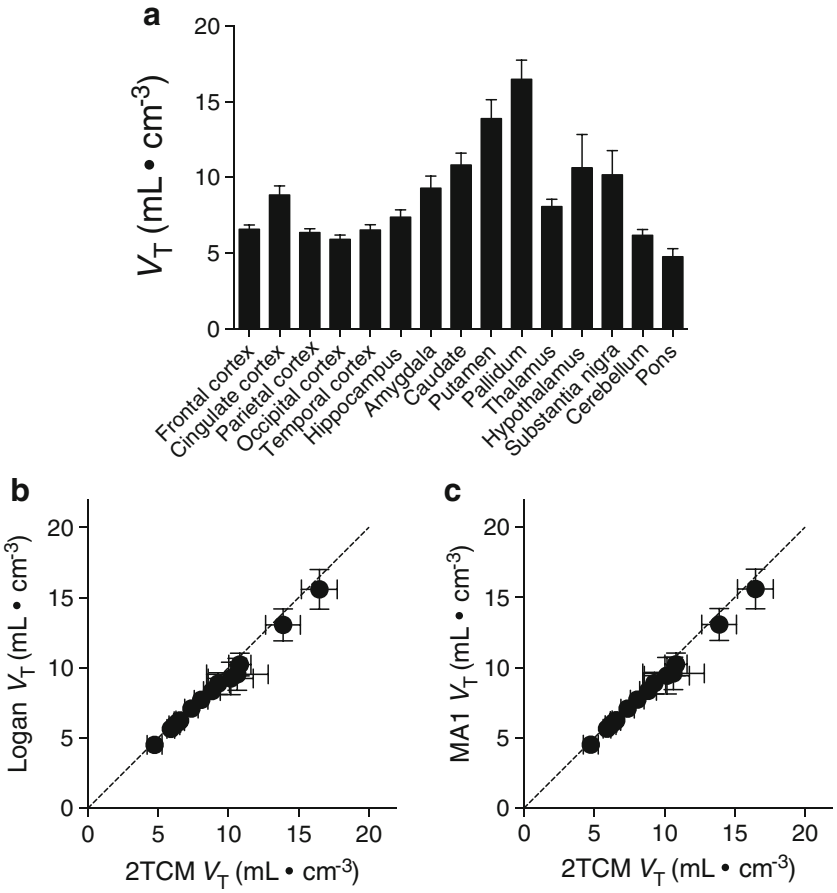

Fig. 5 **a** V_T values estimated with the two-tissue compartment model in various regions using 60-min data. **b**, **c** Correlations between V_T values estimated with the two-tissue compartment model and by graphical analyses. The V_T values estimated by the Logan plot (**b**) and MA1 (**c**) are well correlated with the V_T values estimated with the two-tissue compartment model ($r^2 = 1.00$ for both). *Data points* and *error bars* represent the means and SD from eight subjects for each region. The *straight lines* are the lines of identity

of injection) were also observed in the kidneys (peak activity 8.6 % of the injected activity), spleen (3.3 %), heart (2.4 %), and thyroid (0.3 %). Peak activities were reached more slowly and subsequent slow washout was seen in the liver (peak activity 28 % of the injected activity), brain (8.5 %), red marrow (8.2 %), small intestine (4.6 %), pancreas (2.4 %), large intestine (2.2 %), and stomach (1.7 %). Radioactivity accumulated slowly in the urinary bladder. Exponential fitting of cumulative activity in the urinary bladder indicated that 4.4 % of injected activity was excreted via this route at infinite time with a biological half-life of 17 min. The organs with the longest residence time were liver, lungs, and red marrow (Table 1). The organs with the highest radiation doses were the pancreas, kidneys, and liver (Table 2). The effective dose per injected activity was 6.9 ± 0.03 μSv/MBq.

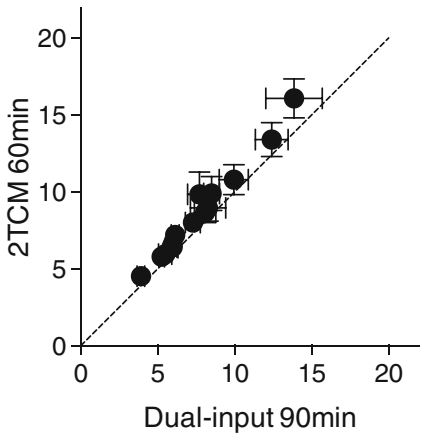

Fig. 6 Correlation between V_T values estimated with the two-tissue and dual-input compartment models. The two-tissue model V_T values from the 60-min scan data correlate very well with the dual-input V_T values from the 90-min scan data ($r^2 = 0.98$). *Data points* and *error bars* represent the means and SD from five subjects. The *straight line* is the line of identity

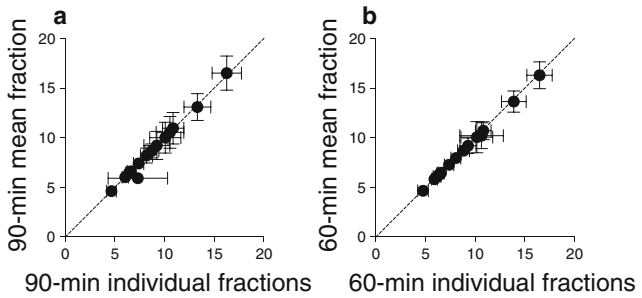

Fig. 7 Correlation between V_T values estimated using the population-mean parent fraction and individual parent fractions. The V_T values match very well for the 90-min (**a**) and 60-min (**b**) data ($r^2 = 0.99$ and 1.00, respectively). *Data points* and *error bars* represent the means and SD from five (**a**) and eight (**b**) subjects. The *straight lines* are the lines of identity

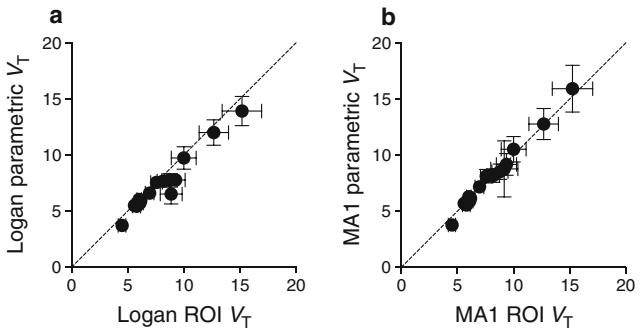

Fig. 8 Correlations between V_T values from ROIs placed on the parametric images and the corresponding V_T values from ROI analysis of graphical analyses. **a** The Logan plot show underestimated V_T values from ROIs placed on the parametric images compared with the corresponding V_T values from ROI analysis (by 0 – 26 %, $r^2 = 0.95$). **b** MA1 does not show such underestimation except in the pons (17 % underestimation in the pons, $r^2 = 0.99$). *Data points* and *error bars* represent the means and SD from ten subjects. The *straight lines* are the lines of identity

Discussion

We evaluated the kinetics and radiation safety profile of [^{11}C]TASP457, a novel PET ligand for histamine H_3 receptors, in human brain. Its uptake was high in the brain especially in regions with a high density of H_3 receptors. The two-tissue compartment model and graphical analyses estimated V_T with excellent identification with 60-min scan data, which represents the known distribution of histamine H_3 receptors. For parametric imaging, MA1 is recommended because of minimal underestimation with small intersubject variability. The current dose of [^{11}C]TASP457 did not cause major safety concerns. The effective dose of [^{11}C]TASP457 is 6.9 μSv/MBq, which would allow multiple injections in the same individual under prevailing permissible-dose guidelines. The advantages of this ligand over the previous ligands include:

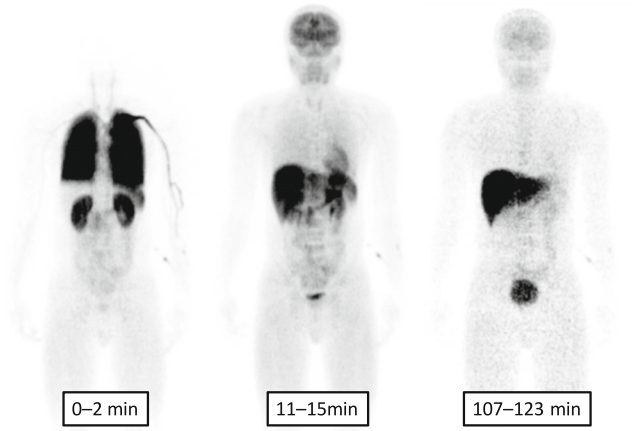

Fig. 9 Whole-body images of a subject obtained at intervals of 0 – 2, 11 – 15, and 107 – 123 min after injection of 181 MBq [^{11}C]TASP457. The images are decay-corrected and displayed using the same gray scale. All coronal slices from each time period were summed to create the images

(1) higher brain penetration than that of [^{11}C]MK-8278, providing equally high specific binding ratios, and (2) faster kinetics than those of [^{11}C]GSK189254, allowing stable quantification of histamine H_3 receptors even in regions with high H_3 receptor densities with a shorter PET acquisition.

In the present study, V_T was estimated with excellent identification and good intersubject variability with 60-min scan data. With the 90-min data, the two-tissue compartment model fitted the time–activity curves better based on multiple criteria. This was confirmed by the graphical analyses with t^* of 30 min indicating that this radioligand is characterized by the two-tissue model rather than the one-tissue model because t^* should theoretically be 0 for one-tissue kinetics. However, [^{11}C]TASP457 90-min brain data did not appear to be appropriate for the estimation of V_T with conventional compartment and graphical analyses for the following reasons. First, V_T estimated using the two-tissue compartment model was unstable in some regions with 90-min data. Second, the time stability analysis with the two-tissue compartment model and MA1 showed that V_T values gradually increased with scan durations of 80 or 70 min and longer (Fig. 4). These two observations may indicate that radiometabolites of [^{11}C]TASP457 gradually enter the brain and contribute to the radioactivity in the brain especially at later time points [23]. We suspect that polar radiometabolites originating from ^{11}C-labeled methyl demethylated from [^{11}C]TASP457 could enter the brain, because a preliminary analysis in mice indicated that about 30 % and 50 % of radioactivity in the brain was from the same radiometabolites seen in humans at 15 and 30 min after injection, respectively (personal communication, K. Kawamura, 2015). However, in humans, metabolism of [^{11}C]TASP457 is much slower than that in mice. Only about 13 % of radioactivity in the plasma was from metabolites in humans compared with about 86 % in mice at 30 min after injection. In addition, graphical analysis showed excellent fitting with the parent only input function (Fig. 3b). Thus, in humans, the potential effect of the metabolite will not be significant if the scan duration is shortened.

We confirmed that 60-min scan data are adequate for measuring binding of [^{11}C]TASP457 to H_3 receptors. First, with 60-min scan data, the time–activity curves were well fitted, and V_T values were well estimated with the two-tissue compartment model and graphical analyses (Logan plot and MA1), consistent with the ligand binding being reversible with moderate affinity. The estimated V_T values had small intersubject variability, and their rank order was consistent with the known distribution of H_3 receptors [5, 24]. Second, the V_T values estimated using the two-tissue compartment model and graphical analysis increased slightly with increasing scan durations beyond 70 min. Third, data from scans shorter than 60-min did not give or gave less stable V_T values because of an insufficient number of data points, especially for graphical analyses, for which t^* is 30 min for this ligand.

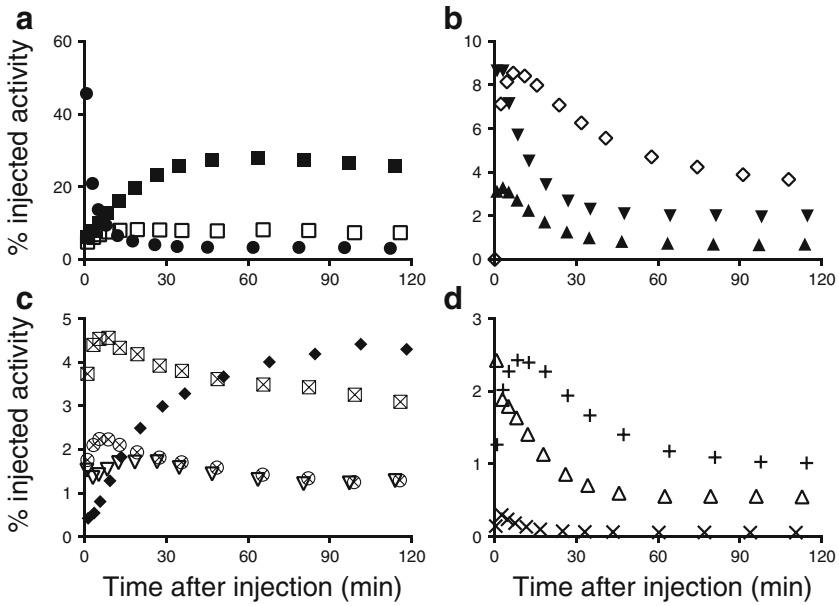

Fig. 10 Decay-corrected time–activity curves for source organs after injection of [^{11}C]TASP457 in three healthy humans. Symbols represent mean radioactivity in the respective organs indicated as percent injected activity. **a** ● lungs, ■ liver, □ red marrow; **b** ◊ brain, ▼ kidney, ▲ spleen; **c** ⊠ small intestine, ◆ urinary bladder, ⊗ large intestine, ▽ stomach; **d** + pancreas, △ heart, × thyroid

To further confirm the adequacy of V_T values estimated using the two-tissue compartment model from the 60-min scan data, we evaluated the correlation between the V_T values from two-tissue compartment and those from the dual-input compartment models, the latter accounting for the contribution of the metabolite brain activity. If the contribution of the metabolite is significant, the former V_T values would be expected to be biased because the metabolite contribution is ignored in the former model [14, 20]. The V_T values from the two-tissue model from the 60-min scan data correlated very well with the dual-input V_T values (Fig. 6), suggesting that the contribution of the metabolite brain activity is relatively minor in magnitude and for practical purposes,

Table 1 Residence times of source organs determined from body imaging with [^{11}C]TASP457

Organ	Residence time (h)
Brain	0.0321 ± 0.0029
Thyroid	0.0006 ± 0.0001
Lungs	0.0464 ± 0.0003
Heart wall	0.0051 ± 0.0001
Liver	0.0952 ± 0.0049
Pancreas	0.0100 ± 0.0003
Spleen	0.0091 ± 0.0059
Stomach	0.0071 ± 0.0031
Large intestine	0.0092 ± 0.0029
Small intestine	0.0199 ± 0.0013
Kidney	0.0205 ± 0.0001
Red marrow	0.0372 ± 0.0032
Urinary bladder	0.0114 ± 0.0021
Remainder of body	0.1883 ± 0.0109

Values are means ± SD from three subjects

Table 2 Radiation dosimetry estimates for [^{11}C]TASP457 in standard reference man

Organ	Dose (μSv/MBq)
Adrenals	3.7 ± 0.1
Brain	7.6 ± 0.6
Breasts	1.6 ± 0.0
Gallbladder wall	4.3 ± 0.1
Lower large intestine wall	6.1 ± 1.2
Small intestine	8.1 ± 0.4
Stomach wall	6.6 ± 1.2
Upper large intestine wall	5.4 ± 0.8
Heart wall	6.7 ± 0.9
Kidneys	20.4 ± 0.4
Liver	17.0 ± 0.9
Lungs	12.5 ± 1.0
Muscle	1.8 ± 0.0
Ovaries	2.6 ± 0.1
Pancreas	27.4 ± 3.7
Red marrow	5.7 ± 0.2
Osteogenic cells	4.6 ± 0.2
Skin	1.3 ± 0.0
Spleen	15.0 ± 6.2
Testes	1.4 ± 0.1
Thymus	1.9 ± 0.0
Thyroid	7.9 ± 1.2
Urinary bladder wall	9.3 ± 1.0
Uterus	2.5 ± 0.1
Effective dose	6.9 ± 0.0

Values are means ± SD from three subjects

a 60-min scan duration is adequate and the metabolite contribution can be ignored in the data analysis.

Our data suggest that for the quantification of [^{11}C]TASP457, MA1 with 60-min data would be appropriate both for ROI analysis and parametric imaging. In the ROI analysis, V_T values estimated with graphical analyses (Logan plot and MA1) showed very good correlations with slight underestimation with those estimated using two-tissue compartment model analysis. In parametric imaging, which allows voxel-based analysis, underestimation of V_T values from the Logan plot was larger because of high noise in the voxel-based time–activity curves than the values from ROI analysis, especially in small regions (Fig. 7a). The values from MA1, which is known to be robust to noise [19], were not underestimated in most regions and the use of this method did not increase intersubject variability except in the substantia nigra (Fig. 7b).

[^{11}C]TASP457 showed slow metabolism in the plasma (Fig. 1b), and the measurement of the fraction was unstable especially at later time points. However, HPLC analysis was successfully performed for 50 – 60 min in nine of ten subjects. Thus, determination of parent fractions should not pose any major difficulty considering that 60-min data (not 90-min data) acquisition is adequate for this ligand. For parametric imaging, we used the time-course of parent fractions from an average of ten subjects to estimate the arterial input function for each subject. This procedure may increase intersubject variability if the estimated arterial input function is not sufficiently accurate. However, we found that individual variation in the parent fraction was modest (Fig. 1b), and V_T values estimated with both the compartment model analysis and graphical analyses showed good intersubject variability (Fig. 8). However, use of the population-mean parent fraction requires caution when it is applied to patients and/or subjects under drug treatment because metabolism of the ligand under such conditions might be quite different from that under normal conditions without the presence of drugs.

Intravenous injection of [^{11}C]TASP457 appeared to be safe and its effective dose was modest. We estimated the radiation burden of [^{11}C]TASP457 to have an effective dose of 6.9 μSv/MBq, which is modest for a ^{11}C-labeled radioligand [25] and would allow multiple injections in the same individual under the prevailing maximum recommended dose guidelines [21]. Under the guidelines of the Radioactive Drug Research Committees operating in the USA (FDA 21 CFR 361.1), the maximal injectable activity would be 1.8 GBq per single administration and 5.5 GBq per year based on the dose to the pancreas (<50 mSv per single administration and 150 mSv per year). Under the regulations of the US Nuclear Regulatory Commission, the maximal injectable activity would be 7.2 GBq per year (<50 mSv per year). Under the European regulation (European Commission, Radiation protection 99), research subjects in Europe could receive no more than 1.4 GBq per year (<10 mSv per year for a "minor to intermediate" increase in risk). Thus, the radiation absorbed doses reported in the current study would allow multiple injections of current doses for brain imaging under all the guidelines.

Conclusion

[^{11}C]TASP457 is a useful novel PET ligand for investigating the density of histamine H_3 receptors in human brain. The two-tissue compartment model and graphical analyses estimated V_T with excellent identification with 60-min scan data, which represents the known distribution of histamine H_3 receptors. For parametric imaging, MA1 is recommended because of minimal underestimation with small intersubject variability. The effective dose of [^{11}C]TASP457 is 6.9 μSv/MBq, which would allow multiple injections in the same individual under prevailing permissible dose guidelines.

Acknowledgments We thank the radiology technologists of the PET Department and members of the Clinical Neuroimaging Team for their support with PET scans, Kazuko Suzuki and Shizuko Kawakami for their assistance as clinical coordinators, Hiromi Sano for her support with MRI scans, the staff of the Molecular Probe Program for radioligand synthesis and metabolite analysis, and Atsuo Waki and his team for quality assurance of the radioligand. The precursor and standard of [^{11}C]TASP457 for this study were provided by Taisho Pharmaceutical Co., Ltd.

Compliance with ethical standards

Funding This study was supported in part by Grants-in-Aid for Scientific Research on Innovative Areas (23111009, 26119531, 26118518) from the Ministry of Education, Culture, Sports, Science and Technology, Japan, Health Labour Sciences Research Grant H25-Seishin-Jituyouka(Seishin)-Ippan-001 from the Ministry of Health, Labour and Welfare, Japan, and the Brain Mapping by Integrated Neurotechnologies for Disease Studies from the Japan Agency for Medical Research and Development.

Conflicts of interest Y.K., K.T., S.K., M.H. and T.S. are involved in joint research and/or a clinical trial sponsored by Taisho Pharmaceutical Co., Ltd. M.H. and T.S. hold a patent for [^{11}C]TASP457 and related chemicals as H_3 ligands (Japan patent JP2014-47209A).

Ethical approval All procedures performed in studies involving human participants were in accordance with the ethical standards of the institutional and/or national research committee and with the ethical standards laid down in the 1964 Declaration of Helsinki and its later amendments or comparable ethical standards.

Informed consent Informed consent was obtained from all individual participants included in the study.

References

1. Arrang JM, Garbarg M, Schwartz JC. Auto-inhibition of brain histamine release mediated by a novel class (H_3) of histamine receptor. Nature. 1983;302:832–7.

2. Haas H, Panula P. The role of histamine and the tuberomamillary nucleus in the nervous system. Nat Rev Neurosci. 2003;4:121–30.
3. Goodchild RE, Court JA, Hobson I, Piggott MA, Perry RH, Ince P, et al. Distribution of histamine H_3-receptor binding in the normal human basal ganglia: comparison with Huntington's and Parkinson's disease cases. Eur J Neurosci. 1999;11:449–56.
4. Esbenshade TA, Browman KE, Bitner RS, Strakhova M, Cowart MD, Brioni JD. The histamine H_3 receptor: an attractive target for the treatment of cognitive disorders. Br J Pharmacol. 2008;154: 1166–81.
5. Ashworth S, Rabiner EA, Gunn RN, Plisson C, Wilson AA, Comley RA, et al. Evaluation of ^{11}C-GSK189254 as a novel radioligand for the H_3 receptor in humans using PET. J Nucl Med. 2010;51:1021–9.
6. Ashworth S, Berges A, Rabiner EA, Wilson AA, Comley RA, Lai RYK, et al. Unexpectedly high affinity of a novel histamine H_3 receptor antagonist, GSK239512, in vivo in human brain, determined using PET. Br J Pharmacol. 2014;171:1241–9.
7. Jucaite A, Takano A, Boström E, Jostell K-G, Stenkrona P, Halldin C, et al. AZD5213: a novel histamine H_3 receptor antagonist permitting high daytime and low nocturnal H_3 receptor occupancy, a PET study in human subjects. Int J Neuropsychopharmacol. 2013;16:1231–9.
8. Van Laere KJ, Sanabria-Bohórquez SM, Mozley DP, Burns DH, Hamill TG, Van Hecken A, et al. ^{11}C-MK-8278 PET as a tool for pharmacodynamic brain occupancy of histamine 3 receptor inverse agonists. J Nucl Med. 2014;55:65–72.
9. Medhurst AD, Atkins AR, Beresford IJ, Brackenborough K, Briggs MA, Calver AR, et al. GSK189254, a novel H_3 receptor antagonist that binds to histamine H_3 receptors in Alzheimer's disease brain and improves cognitive performance in preclinical models. J Pharmacol Exp Ther. 2007;321:1032–45.
10. Koga K, Maeda J, Tokunaga M, Hanyu M, Kawamura K, Ohmichi M, et al. Development of TASP0410457 (TASP457), a novel dihydroquinolinone derivative as a PET radioligand for central histamine H_3 receptors. EJNMMI Res. 2016. doi:10.1186/s13550-016-0170-2.
11. Wardak M, Wong KP, Shao W, Dahlbom M, Kepe V, Satyamurthy N, et al. Movement correction method for human brain PET images: application to quantitative analysis of dynamic ^{18}F-FDDNP scans. J Nucl Med. 2010;51:210–8.
12. Innis RB, Cunningham VJ, Delforge J, Fujita M, Gjedde A, Gunn RN, et al. Consensus nomenclature for in vivo imaging of reversibly binding radioligands. J Cereb Blood Flow Metab. 2007;27: 1533–9.
13. Akaike H. A new look at the statistical model identification. IEEE Trans Automat Contr. 1974;19:716–23.
14. Fujita M, Seibyl JP, Verhoeff NP, Ichise M, Baldwin RM, Zoghbi SS, et al. Kinetic and equilibrium analyses of [^{123}I]epidepride binding to striatal and extrastriatal dopamine D_2 receptors. Synapse. 1999;34:290–304.
15. Hawkins RA, Phelps ME, Huang SC. Effects of temporal sampling, glucose metabolic rates, and disruptions of the blood–brain barrier on the FDG model with and without a vascular compartment: studies in human brain tumors with PET. J Cereb Blood Flow Metab. 1986;6:170–83.
16. Carson RE. Parameters estimation in positron emission tomography. In: Phelps ME, Mazziotta JC, Schelbert H, editors. Positron emission tomography and autoradiography: principle applications for the brain and the heart. New York: Raven Press; 1986. p. 347–90.
17. Logan J, Fowler JS, Volkow ND, Wolf AP, Dewey SL, Schlyer DJ, et al. Graphical analysis of reversible radioligand binding from time-activity measurements applied to [*N*-^{11}C-methyl]-(−)-cocaine PET studies in human subjects. J Cereb Blood Flow Metab. 1990;10:740–7.
18. Logan J, Fowler JS, Volkow ND, Ding Y-S, Wang G-J, Alexoff DL. A strategy for removing the bias in the graphical analysis method. J Cereb Blood Flow Metab. 2001;21:307–20.
19. Ichise M, Toyama H, Innis RB, Carson RE. Strategies to improve neuroreceptor parameter estimation by linear regression analysis. J Cereb Blood Flow Metab. 2002;22:1271–81.
20. Ichise M, Fujita M, Seibyl JP, Verhoeff NP, Baldwin RM, Zoghbi SS, et al. Graphical analysis and simplified quantification of striatal and extrastriatal dopamine D_2 receptor binding with [^{123}I]epidepride SPECT. J Nucl Med. 1999;40:1902–12.
21. Kimura Y, Ito H, Shiraishi T, Fujiwara H, Kodaka F, Takano H, et al. Biodistribution and radiation dosimetry in humans of [^{11}C]FLB 457, a positron emission tomography ligand for the extrastriatal dopamine D_2 receptor. Nucl Med Biol. 2014;41:102–5.
22. Stabin MG, Sparks RB, Crowe E. OLINDA/EXM: the second-generation personal computer software for internal dose assessment in nuclear medicine. J Nucl Med. 2005;46:1023–7.
23. Terry G, Liow J-S, Chernet E, Zoghbi SS, Phebus L, Felder CC, et al. Positron emission tomography imaging using an inverse agonist radioligand to assess cannabinoid CB_1 receptors in rodents. Neuroimage. 2008;41:690–8.
24. Hamill TG, Sato N, Jitsuoka M, Tokita S, Sanabria S, Eng W, et al. Inverse agonist histamine H3 receptor PET tracers labelled with carbon-11 or fluorine-18. Synapse. 2009;63:1122–32.
25. Zanotti-Fregonara P, Innis RB. Suggested pathway to assess radiation safety of ^{11}C-labeled PET tracers for first-in-human studies. Eur J Nucl Med Mol Imaging. 2012;39:544–7.